Correction date March 8, 2021

Melting phase relation of Fe-bearing Phase D up to the uppermost lower mantle

Chaowen Xu*[1,2,3,4], Toru Inoue[1,5,6], Jing Gao[7], Masamichi Noda[1,5,6], Sho Kakizawa[1,5,6]

[1] Geodynamics Research Center, Ehime University, 2-5 Bunkyo-cho, Matsuyama 790-8577, Japan

[2] Institute of Earthquake Forecasting, China Earthquake Administration (CEA,) Beijing, China

[3] The United Laboratory of High-Pressure Physics and Earthquake Science, China Earthquake Administration (CEA,) Beijing, China

[4] Key Laboratory of Earth and Planetary Physics, Institute of Geology and Geophysics, Chinese Academy of Sciences, Beijing, China

[5] Department of Earth and Planetary Systems Science, Hiroshima University, 1-3-1 Kagamiyama, Higashi-Hiroshima 739-8526, Japan

[6] Hiroshima Institute of Plate Convergence Region Research (HiPeR), Hiroshima University, Higashi-Hiroshima, Hiroshima 739-8526, Japan

[7] State Key Laboratory of Lithospheric Evolution, and Institutions of Earth Science, Institute of Geology and Geophysics, Chinese Academy of Sciences, Beijing, China

* Corresponding author: Chaowen Xu (dkchaowen@126.com)

This is the peer-reviewed, final accepted version for American Mineralogist, published by the Mineralogical Society of America.
The published version is subject to change. Cite as Authors (Year) Title. American Mineralogist, in press.
DOI: https://doi.org/10.2138/am-2021-7907. http://www.minsocam.org/

Abstract

Dense hydrous magnesium silicates (DHMSs) are considered important water carriers in the deep Earth. Due to the significant effect of Fe on the stability of DHMSs, Fe-bearing Phase D (PhD) deserves much attention. However, few experiments have been conducted to determine the stability of PhD in different bulk compositions. In this study, we provide experimental constraints for the stability of PhD in the AlOOH-FeOOH-$Mg_{1.11}Si_{1.89}O_6H_{2.22}$ system between 18 and 25 GPa at 1000-1600 ºC, corresponding to the *P-T* conditions of the mantle transition zone and uppermost lower mantle.

Fe^{3+}-bearing PhD was synthesized from the FeOOH-$Mg_{1.11}Si_{1.89}O_6H_{2.22}$ binary system with two different Fe^{3+} contents. The resultant Al, Fe^{3+}-bearing compositions are close to analog specimens of the fully oxidized mid-ocean ridge basalt (MORB) and pyrolite in the AlOOH-FeOOH-$Mg_{1.11}Si_{1.89}O_6H_{2.22}$ ternary system. The substitution mechanism of Fe is shown to be dependent on pressure, and Fe^{3+} occupies both Mg and Si sites in PhD at pressures below 21 GPa. In contrast, Fe^{3+} only occupies Si site at pressures exceeding 21 GPa. The presence of Fe^{3+} results in a slight reduction in the thermal stability field of PhD in the FeOOH-$Mg_{1.11}Si_{1.89}O_6H_{2.22}$ system in comparison to Mg-bearing, Fe-free PhD. In contrast, Al, Fe^{3+}-bearing PhD is more stable than Mg-bearing PhD in both MORB and pyrolite compositions. In this regard, Al, Fe^{3+}-bearing PhD could act as a long-term water reservoir during subduction processes to the deep mantle.

1. Introduction

Water is one of the most important volatiles, and so it plays a crucial role in the

geochemical and geophysical evolution of the Earth. Even a small amount of water may significantly change the physical and chemical properties of the Earth's interior. For example, the presence of water decreases the melting temperature of minerals and changes seismic wave velocity and rheological behavior, thereby influencing the thermodynamic processes of the mantle (Kavner, 2003; Komabayashi and Omori, 2006; Xu et al., 2020). It has previously been found that a series of dense hydrous magnesium silicates (DHMSs), such as Phase A (PhA), Phase E (PhE), Superhydrous phase B (SUB), Phase D (PhD), and Phase H (PhH) are promising water hosts within the context of subduction in the deep Earth (Kawamoto et al., 1996; Ohtani et al., 2001a; Litasov and Ohtani, 2003; Komabayashi et al., 2005; Nishi et al., 2014). The-stability of these phases is, therefore, key to unraveling water recycling throughout the planet over geological time scales.

PhD was identified by Liu (1987) as a new DHMS resulting from the breakdown of serpentine under high *P*-*T* conditions. The ideal chemical formula of PhD is $MgSi_2H_2O_6$, however, PhD exhibits non-stoichiometry with regards to the Mg/Si ratio, which varies from 0.55 to 0.71, and the H content, which varies from 2 to 3.4 per formula unit (Frost and Fei, 1999). PhD also exists as a solid solution via Mg→Fe, Mg+Si→2Al, and Mg+Si→$2Fe^{3+}$ substitution mechanisms. It has trigonal symmetry ($P\bar{3}1m$) with SiO_6 and MgO_6 octahedra alternately stacked along the c-axis (Kudoh et al., 1997; Yang et al., 1997). PhD is potentially a stable phase in hydrous peridotite among DHMSs at the upper part of the lower mantle, allowing it to play a key role in the transportation of water, subsequently transforming to Phase H (PhH) at 50 GPa (Nishi et al., 2014). Earlier experimental results suggest that additional Al_2O_3 may increase the region of thermal stability of PhD (Ghosh

and Schmidt, 2014; Xu and Inoue, 2019a), and Al-rich PhD could remain stable up to 2000 ºC at 25 GPa (Pamato et al., 2015). However, there is no clear consensus in the literature regarding the effect of Fe substitution on the stability of PhD. Ghosh and Schmidt (2014) suggested that the maximum stability limit of PhD is between 1350 ºC and 1400 ºC at 22–24 GPa in both the FeO-MgO-Al_2O_3-SiO_2-H_2O (FMASH) and MSH systems, i.e., 200 ºC lower than that of the MASH system. However, compared with the MSH system between 18–23 GPa, Ganskow and Langenhorst (2014) argued that the presence of Fe^{2+} would increase the stability of PhD in the FMASH system up until 1450 ºC at 20.5 GPa. Beyond these studies, there is a paucity of research on the effect of Fe on the stability of DHMSs. Fe is an abundant and important element in both pyrolite and mid-ocean ridge basalts (MORB), and the presence of Fe may significantly change the stability of PhD and its water solubility. Additionally, the stability of PhD containing Fe and Al simultaneously, which is closer in composition to pyrolite or MORB, is unknown.

The oxide hydroxides AlOOH and FeOOH are common minerals in sediments (Otte et al., 2009; Panero and Stixrude, 2004). At low pressures, AlOOH has two polymorphic structures; diaspora (α-AlOOH, space group *Pbnm*) and boehmite (γ-AlOOH, *Amam*), which transform to δ-AlOOH (*P*21*nm*) at around 17 GPa and 1000 ºC (Ohtani et al., 2001b), and subsequently to pyrite-type structures at 170 GPa (*Pa*-3) (Tsuchiya and Tsuchiya, 2011). At lower pressures, FeOOH has three polymorphic structures, i.e., goethite (α-FeOOH iso-structure with α-AlOOH), akaganeite (β-FeOOH, I4/m), and lepidcrocite (γ-FeOOH, *Cmcm*). Goethite transforms to ε-FeOOH (isostructural with δ-AlOOH) at pressures above 5 GPa at 200 ºC (Gleason et al., 2008), which then transforms into pyrite-type FeOOH at

86 pressures between 60-90 GPa and temperatures exceeding 1227 ºC (Nishi et al., 2017).
87 Experimental results show that δ-AlOOH, ε-FeOOH, and PhH ($MgSiH_2O_4$) may form solid
88 solutions in the Earth's deep lower mantle (Sano et al., 2008; Ohira et al., 2014; Ohtani et
89 al., 2014; Nishi et al., 2017; Xu et al., 2019a). However, the stability of δ-AlOOH and
90 ε-FeOOH in the Mg, Si-bearing systems under transition zone conditions has not been as
91 well investigated.

92 In this study, we determined the effect of Fe^{3+} on the stability of PhD in the
93 FeOOH-$Mg_{1.11}Si_{1.89}O_6H_{2.22}$ system at pressures between 18 and 25 GPa and temperatures
94 between 1000 and 1600 ºC. Additionally, we determined the stability of PhD with
95 intermediate Al and Fe^{3+} content in the AlOOH-FeOOH-$Mg_{1.11}Si_{1.89}O_6H_{2.22}$ system whose
96 composition is similar to pyrolite and MORB in the natural system. We simultaneously
97 clarified the effect of Mg and Si on the stability of AlOOH-FeOOH phases for transition
98 zone conditions, as Mg and Si change the symmetry of δ-AlOOH (Komatsu et al., 2011),
99 which might influence the stability of the phase.

100

101 **2. Experiment**

102 To prepare PhD with a homogeneous composition close to $Mg_{1.11}Si_{1.89}O_6H_{2.22}$, we
103 used a mixture of $Mg(OH)_2$ + SiO_2 in appropriate stoichiometry. To study the effect of Fe^{3+}
104 content on the stability of PhD, 15.0 wt% and 8.0% wt% of α-FeOOH + $Mg_{1.11}Si_{1.89}O_6H_{2.22}$
105 respectively, were adopted. Furthermore, 5.7 wt% of AlOOH (Al_2O_3 + $Al(OH)_3$ in
106 appropriate stoichiometry) + 9.4 wt% of α-FeOOH (4.0 wt% A_2O_3, 8.4 wt% Fe_2O_3) +

107 $Mg_{1.11}Si_{1.89}O_6H_{2.22}$ and 16.0 wt% of AlOOH + 8.8 wt% of α-FeOOH (13.6 wt% A_2O_3, 7.9
108 wt% Fe_2O_3) + $Mg_{1.11}Si_{1.89}O_6H_{2.22}$ were utilized, respectively, whose Al and Fe composition
109 were close to pyrolite (4.3 wt% A_2O_3, 8.0 wt% Fe_2O_3) and MORB (15.3 wt% A_2O_3, 10.4
110 wt% Fe_2O_3) (Ringwood, 1975; Hofmann, 1988).

111 The experiments were conducted at pressures of 18–25 GPa and temperatures from
112 1000 ºC to 1600 ºC using a MA-8 type apparatus (ORANGE-1000) at the Geodynamics
113 Research Center (GRC) of Ehime University, Japan. The pressure was calibrated at room
114 temperature through the diagnostic changes in the electrical resistances of ZnTe (9.6 and
115 12.0 GPa), ZnS (15.5 GPa), GaAs (18.3 GPa), and GaP (23.0 GPa), induced by the
116 semiconductor-metal phase transitions at high pressures. Tungsten carbide cubes with a
117 truncation edge length (TEL) of 4 mm were combined with Cr-doped MgO-octahedra with
118 an edge length of 10 mm (10/4 assemblage). Preformed pyrophyllite gaskets were used
119 between the anvils, and lanthanum chromate ($LaCrO_3$) was used as the heater. The sample
120 was sealed by welding it in a gold capsule to prevent water loss during the experiment. The
121 temperature was monitored by a $W_{97}Re_3$-$W_{75}Re_{25}$ thermocouple, and the thermocouple emf
122 was not corrected for the effect of pressure. The samples were recovered when the pressure
123 was released slowly over 720 minutes.

124 The recovered products of each experimental run were mounted in epoxy resin and
125 polished to undergo phase identification and composition analysis. The phase assemblages
126 were identified by a micro-focus X-ray diffractometer (Rigaku MicroMax-007HF) using
127 Cu Kα radiation. For electron microscopic measurements, the samples were coated with
128 carbon. The micro-textures and composition were obtained using a field emission scanning

129 electron microscope (FESEM, JEOL JSM7000F) combined with an energy dispersive
130 X-ray spectrometer (EDS, Oxford Instruments X-MaxN) with the working parameters of 15
131 kV, 1 nA, and collection times of 30–50 s. Olivine and alumina were employed as the
132 standards for Mg, Al, Si, and Fe. The Aztec software (version 2.4, Oxford Instruments
133 Nanotechnology Tools Ltd) was used to determine the composition by EDS. For more
134 detailed experimental information, please refer to Text S1.

135

136 **3. Results**

137 **3.1 Phase relations**

138 Figure 1 shows the back-scattered electron (BSE) images of typical experimental run
139 products, and a summary of the quenched phase assemblages is given in Table 1. The phase
140 assemblages are simple and include PhD, Fe_2O_3, bridgmanite, garnet, stishovite, and melt.
141 A trace amount of ringwoodite was also observed.

142 At 25 GPa and 1200 ºC, the BSE image (shown in Figure 1a) shows the presence of
143 PhD and Fe_2O_3 in bright and dark colors, respectively, with higher Fe^{3+} content in the
144 FeOOH-$Mg_{1.11}Si_{1.89}O_6H_{2.22}$ system. The same phase assemblage was observed under
145 equivalent *P-T* conditions with lower Fe^{3+} content in the FeOOH-$Mg_{1.11}Si_{1.89}O_6H_{2.22}$,
146 system as shown in Figure 1b. This suggests that the solubility of Fe^{3+} in PhD was quite
147 low. At elevated temperatures, phase assemblages with both higher and lower Fe^{3+} content
148 look the same, except that excess Fe_2O_3 was identified in the system with higher Fe^{3+}
149 content, as shown in Figures. 1c and 1d. In the AlOOH-FeOOH-$Mg_{1.11}Si_{1.89}O_6H_{2.22}$ ternary

system, garnet, stishovite, and melt were found with both MORB and pyrolite-type compositions at 21 GPa. Additionally, phase Egg was also observed in the MORB-type composition.

3.1.1 The FeOOH-$Mg_{1.11}Si_{1.89}O_6H_{2.22}$ system

A new PhD phase diagram is shown in Figure 2. At 18 GPa and 1000 ºC, the phase assemblages look similar to each other within both starting compositions. PhD was observed with both higher and lower Fe content, and a trace amount of ringwoodite was identified in the quenched samples. At 20 GPa and 1100 ºC, ringwoodite disappeared with higher iron content. Furthermore, Fe_2O_3 instead of ε-FeOOH formed in some of the quenched samples at pressures of 18 GPa to 25 GPa. Although ε-FeOOH has the same $CaCl_2$-type crystal structure as δ-AlOOH (Ohtani et al., 2001b; Suzuki, 2010), our data indicates that the Fe-rich ε-phase decomposed into Fe_2O_3 + H_2O at all *P-T* conditions in this study. We observe that dehydration of δ-AlOOH occurs at 20 GPa and 1200 ºC, suggesting that the dehydration temperature of ε-FeOOH is lower than that of both δ-AlOOH and Fe^{3+}-bearing PhD, or that the activity of H_2O was too low, or the activity of SiO_2 was too high to stabilize ε-FeOOH.

PhD was observed at 21 GPa and 1100 ºC in both starting compositions, but disappeared at 1300 ºC. At 25 GPa and 1200 ºC, PhD coexisted with Fe_2O_3 in both compositions. When the temperature was increased to 1400 ºC, both phase assemblages transformed into bridgmanite (brg) + stishovite (st) + melt (shown in Figures 1c and 1d).

171 This reaction is the same as the thermodynamic calculation PhD = Brg + St + H_2O reported
172 by Komabayashi and Omori (2006).

173 The highest thermal stability of PhD at 18 GPa, 20 GPa, 21 GPa, and 25 GPa is
174 around 1100 ºC, 1150 ºC, 1200 ºC, and 1350 ºC, respectively, indicating that our results are
175 consistent with a positive Clapeyron slope in a Fe^{3+}-bearing system. Such a positive slope
176 had been previously determined by Frost and Fei (1998) in the Fe-free system, and by
177 Ghosh and Schmidt (2014) in the Al, Fe^{2+}-bearing system, however, our results are
178 different from the Fe^{2+}-bearing and Al, Fe^{2+}-bearing systems suggested by Ganskow and
179 Langenhorst (2014).

180

181 *3.1.2 The AlOOH-FeOOH-$Mg_{1.11}Si_{1.89}O_6H_{2.22}$ system*

182 The phase relation is shown in Figure 2. At 21 GPa and 1300 ºC, Fe-bearing PhD was
183 observed in the starting compositions. Nevertheless, a small amount of Fe_2O_3 appeared in
184 the pyrolite-type composition as shown in Figures 1e and 1f. Our results indicate that Al_2O_3
185 enhances the solubility of Fe^{3+} in PhD. In addition, the added Al_2O_3 in the starting
186 composition has a great impact on the stability field of PhD at 21 GPa, causing the stability
187 boundary to shift to around 1400 ºC. At 1500 ºC, PhD decomposed to Gt + St + melt,
188 whereas hydrous phase Egg was observed in the MORB-type starting composition at high
189 temperatures (Figures 1g and 1h). The stability condition of phase Egg in this study is
190 consistent with that of previous reports (Sano et al., 2004; Fukuyama et al., 2017), implying
191 that phase Egg is a potential hydrous phase at high temperatures around the mantle

192 transition zone.

193

194 **3.2. Mineral compositions**

195 *3.2.1. Mineral chemistry*

196 Representative mineral compositions are summarized in Table S1. In the FeOOH-
197 $Mg_{1.11}Si_{1.89}O_6H_{2.22}$ binary system, the content range of MgO and SiO_2 in PhD is very
198 narrow, i.e., from 20.44 to 22.91 wt% and 58.83 to 62.26 wt%, respectively, in the high
199 Fe^{3+} content system, and 20.27 to 21.79 wt% MgO and 60.59 to 63.58 wt% SiO_2 in the low
200 Fe^{3+} content system between 18–25 GPa. The H_2O content in the PhD was calculated from
201 the deficit of the total weight percent in the EDS analysis for an average of 12.19 wt% and
202 12.02 wt%, respectively. The relationship between the pressure and Fe_2O_3 content in PhD is
203 shown in Figure 3, which clearly shows that, with increasing pressure, Fe content decreases
204 below 21 GPa, and then slightly increases up to 25 GPa. This trend was consistent with the
205 previous result obtained by Ganskow and Langenhorst (2014), as shown in Figure 3,
206 although the starting composition in that study showed very high FeO content (37.9 wt%).
207 Compared with pressure, temperature seems to have little effect on the solubility of Fe^{3+} in
208 PhD. In the AlOOH-FeOOH-$Mg_{1.11}Si_{1.89}O_6H_{2.22}$ ternary system, both MgO and SiO_2
209 decreased in PhD with increasing pressure. By contrast, the Fe^{3+} content increased in both
210 the pyrolite and MORB-type compositions compared with the FeOOH-$Mg_{1.11}Si_{1.89}O_6H_{2.22}$
211 binary system, as shown in Figure 3.

212 At higher temperatures, garnet is able to stabilize in the FeOOH-$Mg_{0.5}Si_{0.5}OOH$

binary system. A large amount of garnet was found at 21 GPa and 1500 ºC, which contains 22.07 and 21.59 wt% of Al_2O_3 in the MORB- and pyrolite-type starting compositions, respectively. The calculated Mg/Si ratio of the ringwoodite that appeared in the FeOOH-$Mg_{1.11}Si_{1.89}O_6H_{2.22}$ binary system is less than 2, implying the incorporation of H_2O via the substitution mechanism $Mg^{2+}= 2H^+$. The H_2O content in ringwoodite estimated by EDS total deficit is 1.5 wt% at 21 GPa and 1300 ºC in MORB-type compositions, and 1.3 wt% at 20 GPa and 1100 ºC in pyrolite-type compositions. Based on previous experiments, the H_2O solubility in ringwoodite was as high as 3.1 wt%, meaning that the mantle transition zone may be water-saturated (Inoue et al., 1995; Fei et al., 2017), indicating that ringwoodite is a potential water reservoir within the mantle transition zone.

3.2.2. Lattice parameters

The relationship between unit cell volume of PhD in the FeOOH-$Mg_{1.11}Si_{1.89}O_6H_{2.22}$ binary system and Mg/Si is shown in Figure 4, where there are distinctly different relationships between Mg/Si and unit cell volumes between 18 and 20 GPa compared to 25 GPa. The unit cell volume slightly decreased with increased pressure from 18 to 20 GPa, and almost the same Mg/Si ratios were obtained within this pressure range. The volume change is consistent with the Fe_2O_3 content in PhD below 21 GPa, as shown in Figure 3. The decreased Fe_2O_3 content may lead to a decrease in volume due to the larger ion size of Fe^{3+} compared with Mg and Si. However, the unit cell volume increases even with low Fe_2O_3 content at 25 GPa, and the Mg/Si ratio also increased at the same pressure. This phenomenon is probably related to different substitution mechanisms of Fe^{3+} in PhD. The crystal structure of PhD is rather simple, as all the Mg and Si occupy octahedral sites.

When the pressure is below 21 GPa, Tschermak-type substitution ($Mg^{2+}+Si^{4+}=2Fe^{3+}$) occurs in both Mg and Si sites. That is, the decrease of Fe^{3+} content would lead to a decrease in volume. By contrast, Fe^{3+} only occupied Si sites at elevated pressures ($Si^{4+}=Fe^{3+}+H^{+}$), leading to an increase of volume even with low Fe_2O_3 content. For more information, please refer to Figure S1. Of course, there may exist another possibility that the coexisting phases with PhD will influence both the Mg/Si ratios and the substitution mechanism. Further studies will be required to clarify this issue.

4. Discussion

4.1 The stability of Fe-bearing PhD in the mantle

The stability of PhD was analyzed in the MgO-SiO_2-H_2O (MSH) system for pressure ranging from 16 to 25 GPa and temperature from 900 to 1400 ºC by Frost and Fei (1998). It can be seen from the results that PhD has a wide stability region ranging from 1000 ºC at 17 GPa to 1400 ºC at 26 GPa. PhD was also investigated in the MgO-Al_2O_3-SiO_2-H_2O (MASH) system by Ghosh and Schmidt (2014), whose results showed that the addition of Al_2O_3 increased the stability field of PhD until 1600 ºC at 24 GPa. It has also been reported that Al-rich PhD could remain stable at temperatures up to 2000°C at 26 GPa (Pamato et al., 2015).

However, there remains significant regarding the effect of Fe on DHMSs, which is important considering that Fe is an abundant element on the Earth. Ghosh and Schmidt (2014) reported that Fe^{2+} decreased the stability of PhD by 200 ºC when adding 4.3 wt% of

256 FeO into reduced FMASH composition compared with the MASH system at pressures
257 between 22 and 24 GPa. By contrast, Ganskow and Langenhorst (2014) observed that Fe^{2+}
258 was available to maintain the stability of PhD of both reduced FMSH and FMASH
259 compositions with a FeO content of 37.9 wt% and 17.9 wt%, respectively. It can be seen
260 that the highest thermal stability is up to 1450 ºC at 20.5 GPa, which is higher compared to
261 the reported thermal stability of Mg-PhD at 1400 ºC and 25 GPa (Frost and Fei, 1998).
262 According to our results, Fe^{3+} slightly destabilizes the thermal stability of PhD when
263 considering PhD with both low (7.2 wt%) and high Fe_2O_3 (13.5 wt%) contents. For
264 example, in the MSH system, PhD was observed at 21.7 GPa and 1300 ºC (Frost and Fei,
265 1998), whereas Fe^{3+}-bearing PhD has already disappeared under the same *P*-*T* conditions in
266 our experiments.

267 Oxygen fugacity plays an important role in the determination of the physical and
268 chemical properties of mantle materials. By controlling the Fe^{3+} or Fe^{2+} content in a mineral,
269 the transport properties can be influenced, including element partitioning, electrical
270 conductivity, and creep (Ryerson et al., 1989; Frost et al., 2001). The minimum $Fe^{3+}/\Sigma Fe$ of
271 the bulk rock ratio is estimated to be 3% under mid-transition zone conditions (Frost and
272 McCammon, 2008), indicating that the oxidation state of the mantle is reduced. However,
273 in the current experiment, we describe extremely oxidized bulk starting compositions, but
274 were unable to determine if oxygen fugacity influences the stability limit of PhD. Previous
275 research has illustrated that even when Fe^{2+} was used in the starting compositions under
276 very reducing redox conditions, a certain amount of Fe^{3+} is still found in the resultant
277 synthesized products (Frost et al., 2004; Saikia et al., 2009). For example, electron

278 energy-loss spectroscopy by Ganskow and Langenhorst (2014) found $Fe^{3+}/\Sigma Fe$ =74% in Fe
279 and Al, Fe^{2+}-bearing PhD, even though they used FeO in their starting material.
280 Additionally, earlier studies have shown that Fe^{2+} tends to partition into ringwoodite rather
281 than PhD under transition zone conditions (Frost et al., 2004; Saikia et al., 2009; Ganskow
282 and Langenhorst, 2014). This means that the gap between the Fe^{3+} contents of the PhD in
283 our experiment and those of previous studies may be negligible under subduction zone
284 conditions. Further experiments have to be conducted to investigate whether oxygen
285 fugacity has an impact on the thermal stability of Fe^{3+}-bearing PhD.

286 Although Fe^{3+}-bearing PhD decomposes at 21 GPa and below 1300 ºC, Al,
287 Fe^{3+}-bearing PhD remains stable above 1300 ºC in both hydrous pyrolite and MORB-type
288 compositions, as shown in Figure 2. Meanwhile, previous studies have suggested that Al
289 preferentially partitions into PhD rather than coexisting wadsleyite, ringwoodite,
290 bridgmanite, and phase H (Bolfan-Casanova et al., 2003; Litasov et al., 2005; Ghosh and
291 Schmidt, 2014; Ohira et al., 2014; Bindi et al., 2015; Pamato et al., 2015). The main factor
292 for this stabilization was attributed to the effect of Al on the stability of PhD. It can be seen
293 from our results that Al could offset the negative effect of Fe^{3+} on the stability of PhD and
294 stabilize it at higher temperatures. Consequently, considering the stabilizing effect of Al, the
295 stability region of Al, Fe^{3+}-bearing PhD should increase.

296

297 **5. Implications**

298 **5.1 Long water reservoir**

299 The stability region of DHMSs has been intensively reported upon by many
300 researchers for simple MSH or MAS systems (Kanzaki, 1991; Kawamoto et al., 1996; Frost
301 and Fei, 1998; Ulmer and Trommsdorff, 1999; Ohtani et al., 2001, 2004; Litasov and
302 Ohtani, 2002; Komabayashi et al., 2005; Komabayashi and Omori, 2006; Ghosh and
303 Schmidt, 2014; Nishi et al., 2014; Pamato et al., 2015; Xu and Inoue, 2019b), where these
304 studies agree that Al drastically increases the thermal stability region of DHMSs. Among
305 the DHMSs, PhD represents an important water carrier from the transition zone to the
306 upper parts of the lower mantle. With the increase in pressure, PhD transforms into a
307 high-pressure polymorph, phase H, at around 48 GPa, which is equivalent to a depth of
308 1,500 km (Nishi et al., 2014). Recent experimental research has shown that Phase H could
309 form a solid solution with δ-AlOOH, and coexist with bridgmanite along slab geotherms,
310 which means that water may be transported to the base of the lower mantle (Ohira et al.,
311 2014).

312 Through the combination of the current experiments and previous results, PhD may be
313 expected to remain stable along the hot subduction zone in both hydrous pyrolite and
314 MORB-type materials, and the increased Fe content may help PhD to sink into deeper
315 regions. Furthermore, if subducting slabs stagnate at the mantle transition zone, Al-rich
316 PhD may transform into phase Egg under *P*-*T* conditions, approximating the mantle
317 geotherm. As subduction continues, some PhD may decompose to bridgmanite, stishovite,
318 and H_2O when present in the uppermost lower mantle. The released water from the
319 breakdown of PhD may cause partial melting and contribute to the observed low-velocity
320 zones at the uppermost lower part of the Japanese subduction zone (Liu et al., 2016).

Additionally, a previous study has suggested that Al-bearing stishovite enhanced (<2.3 wt % Al_2O_3) the substitution of water in stishovite via the mechanism $Al^{3+} + H^{+} = Si^{4+}$ (Pawley et al., 1993). The recovered stishovite, with a Al_2O_3 content of 2.89 wt% and a total weight percent of 98.97 at 21 GPa and 1500°C indicates that water could be held in stishovite even under normal mantle geotherm conditions. Therefore, Al-bearing stishovite is expected to be carried to the lower mantle along the subduction zone in Al-rich bulk compositions (Lin et al., 2020; Nisr et al., 2020) and may transport water with it. Based on these new findings, this study helps to broaden our understanding of the deep-water cycle within the Earth.

ACKNOWLEDGMENTS

We thank Qingyang Hu and Bob Myhill for their constructive comments to improve the quality of the article. This work is supported by the Natural Science Foundation of China (No. 42003050 and No. 42073063), China Postdoctoral Science Foundation (No. 2020M680619), Open Foundation of the United Laboratory of High-Pressure Physics and Earthquake Science (No. 2019HPPES07), Open Foundation of Key Laboratory of Earth and Planetary Physics, Chinese Academy of Sciences (No. DQXX2021-06) and Foundation of the Key Laboratory of Earthquake Forecasting, the Institute of Earthquake Forecasting, CEA (No. 2019IEF0502). C.X. was also supported by Research Fellowships of the Japan Society for the Promotion of Science (JSPS) for Young Scientists (DC2). This work was supported by JSPS KAKENHI Grant Numbers 18J12511 for C.X. and 26247073, 15H05828 and 18H03740 for T.I..

343

344 **References**

345 Anderson, D. (1972) Internal constitution of Mars. Journal of Geophysical Research, 77,
346 789–795, doi: 10.1029/JB077i005p00789.

347 Ballaran, T. B., Frost, D. J., Miyajima, N., and Heidelbach, F. (2010) The structure of a
348 super-aluminous version of the dense hydrous-magnesium silicate phase D. American
349 Mineralogist, 95, 1113–1116, doi: 10.2138/am.2010.3462.

350 Bindi, L., Nishi, M., and Irifune, T. (2015) Partition of al between phase D and phase H at
351 high pressure: results from a simultaneous structure refinement of the two phases
352 coexisting in a unique grain. American Mineralogist, 100, 1637–1640, doi:
353 10.2138/am-2015-5327.

354 Bolfan-Casanova, N., Keppler, H., and Rubie, D. (2003) Water partitioning at 660 km depth
355 and evidence for very low water solubility in magnesium silicate perovskite.
356 Geophysical Research Letters, 30, 169–172, doi: 10.1029/2003GL017182.

357 Fei, H., Yamazaki, D., Sakurai, M., Miyajima, N., and Yamamoto, T. (2017) A nearly
358 water-saturated mantle transition zone inferred from mineral viscosity. Science
359 Advances, 3, e1603024, doi: 10.1126/sciadv.1603024.

360 Frost, D. J., Langenhorst, F., and Aken, P. A. V. (2001) Fe–Mg partitioning between
361 ringwoodite and magnesiowüstite and the effect of pressure, temperature and oxygen

362 fugacity. Physics and Chemistry of Minerals, 28, 455–470, doi:
363 10.1007/s002690100181.

364 Frost, D. J., Liebske, C., Langenhorst, F., McCammon, C. A., Trønnes, R. G., et al. (2004)
365 Experimental evidence for the existence of iron-rich metal in the Earth's lower mantle.
366 Nature, 248, 409–12, doi: 10.1038/nature02413.

367 Frost, D. J., McCammon, C. A. (2008) The redox state of earth's mantle. Annual Review of
368 Earth and Planetary Sciences, 36, 389–420, doi:
369 10.1146/annurev.earth.36.031207.124322.

370 Fukuyama, K., Ohtani, E., Shibazaki, Y., Kagi, H., and Suzuki, A. (2017) Stability field of
371 phase egg, $AlSiO_3OH$ at high pressure and high temperature: possible water reservoir
372 in mantle transition zone. Journal of Mineralogical and Petrological Sciences, 112, 31–
373 35, doi: 10.2465/jmps.160719e.

374 Ghosh, S., Schmidt, M. (2014) Melting of phase D in the lower mantle and implications for
375 recycling and storage of H_2O in the deep mantle. Geochimica et Cosmochimica
376 Acta, 145, 72–88, doi: 10.1016/j.gca.2014.06.025.

377 Gleason, A., Jeanloz, R., and Kunz, M. (2008) Pressure-temperature stability study of
378 FeOOH using X-ray diffraction. American Mineralogist, 93, 1882–1885, doi:
379 10.2138/am.2008.2742.

Hofmann, A. (1988) Chemical differentiation of the Earth: The relationship between mantle, continental crust, and oceanic crust. Earth and Planetary Science Letters, 90, 297–314, doi: 10.1016/0012-821X(88)90132-X.

Inoue, T., Yurimoto, H., and Kudoh, Y. (1995) Hydrous modified spinel, $Mg_{1.75}SiH_{0.5}O_4$: a new water reservoir in the mantle transition region. Geophysical Research Letters, 22, 117–120, doi: 10.1029/94GL02965.

Kavner, A. (2003) Elasticity and strength of hydrous ringwoodite at high pressure. Earth and Planetary Science Letters, 214, 645–654, doi: 10.1016/S0012-821X(03)00402-3.

Kawamoto, T., Hervig, R., and Holloway, J. (1996) Experimental evidence for a hydrous transition zone in the early earth's mantle. Earth and Planetary Science Letters, 142(3), 587–592, doi: 10.1016/0012-821X(96)00113-6.

Komabayashi, T., Hirose, K., Funakoshi, K., and Takafuji, N. (2005) Stability of phase A in antigorite (serpentine) composition determined by in situ x-ray pressure observations. Physics of the Earth and Planetary Interiors, 151, 276–289, doi: 10.1016/j.pepi.2005.04.002.

Komabayashi, T., Omori, S. (2006) Internally consistent thermodynamic data set for dense hydrous magnesium silicates up to 35 GPa, 1600 °C: Implications for water circulation in the Earth's deep mantle. Physics of the Earth and Planetary Interiors, 156, 89–107, doi: 10.1016/j.pepi.2006.02.002.

399 Kudoh, Y., Nagase, T., Mizohata, H., and Ohtani, E. (1997) Structure and crystal chemistry
400 of phase G: A new hydrous magnesium silicate synthesized at 22 GPa and 1050 °C.
401 Geophysical Research Letters, 24, 1051–1054, doi: 10.1029/97GL00875.

402 Lin, Y., Hu, Q., Meng, Y., Walter, M., and Mao, H. K. (2020) Evidence for the stability of
403 ultrahydrous stishovite in earth's lower mantle. Proceedings of the National Academy
404 of Sciences, 117, 184–189, doi: 10.1073/pnas.1914295117.

405 Litasov, K., Ohtani, E. (2003) Stability of various hydrous phases in CMAS pyrolite-H_2O
406 system up to 25 GPa. Physics and Chemistry of Minerals, 30, 147–156, doi:
407 10.1007/s00269-003-0301-y.

408 Liu, L. G. (1987) Effects of H_2O on the phase behavior of the forsterite-enstatite system at
409 high pressures and temperatures and implications for the earth. Physics of the Earth
410 and Planetary Interiors, 49, 142–167, doi: 10.1016/0031-9201(93)90013-Y.

411 Liu, Z., Park, J., and Karato S. (2016) Seismological detection of low-velocity anomalies
412 surrounding the mantle transition zone in Japan subduction zone. Geophysical
413 Research Letters, 43, 2480–2487, doi: 10.1002/2015GL067097.

414 Nishi, M., Irifune, T., Tsuchiya, J., Nishihara, Y., Fujino, K., and Higo, Y. (2014) Stability
415 of hydrous silicate at high pressures and water transport to the deep lower
416 mantle. Nature Geoscience, 7, 224–227, doi: 10.1038/ngeo2074.

417 Nishi, M., Kuwayama, Y., Tsuchiya, J., and Tsuchiya, T. (2017) The pyrite-type
418 high-pressure form of FeOOH. Nature, 547, 205–208, doi: 10.1038/nature22823.

419 Nisr, C., Chen, H., Leinenweber, K., Chizmeshya, A., Prakapenka, V. B., and Prescher, C.,
420 et al. (2020) Large H_2O solubility in dense silica and its implications for the interiors
421 of water-rich planets. Proceedings of the National Academy of Sciences, 117, 9747–
422 9754, doi: 10.1073/pnas.1917448117.

423 Ohira, I., Ohtani, E., Sakai, T., Miyahara, M., Hirao, N., Ohishi, Y., and Nishijima, M.
424 (2014) Stability of a hydrous δ-phase, AlOOH-$MgSiO_2(OH)_2$, and a mechanism for
425 water transport into the base of lower mantle. Earth and Planetary Science Letters, 401,
426 12–17, doi: 10.1016/j.epsl.2014.05.059.

427 Ohtani, E., Toma, M., and Litasov, K. (2001) Stability of dense hydrous magnesium silicate
428 phases and water storage capacity in the transition zone and lower mantle. Physics of
429 the Earth and Planetary Interiors, 124, 105–117, doi:
430 10.1016/S0031-9201(01)00192-3.

431 Otte, K., Pentcheva, R., Schmahl, W., and Rustad, J. (2009) Pressure-induced structural and
432 electronic transitions in FeOOH from first principles. Physical Review B Condensed
433 Matter, 80, 205116, doi: 10.1103/PhysRevB.80.205116.

434 Pamato, M., Myhill, R., Boffa Ballaran, T., Frost, D., Heidelbach, F., and Miyajima, N.
435 (2014) Lower-mantle water reservoir implied by the extreme stability of a hydrous
436 aluminosilicate. Nature Geoscience, 8, 75–79, doi: 10.1038/ngeo2306.

437 Panero, W., Stixrude, L. (2004) Hydrogen incorporation in stishovite at high pressure and
438 symmetric hydrogen bonding in δ-AlOOH. Earth and Planetary Science Letters, 221,
439 421–431, doi: 10.1016/S0012-821X(04)00100-1.

440 Pawley, A., Mcmillan, P., Holloway, J. (1993) Hydrogen in Stishovite, with Implications for
441 Mantle Water Content. Science, 261, 1024–1026, doi: 10.1126/science.261.5124.1024.

442 Ringwood, A. (1975) Composition and Petrology of the Earth's Mantle: New York,
443 McGraw-Hill, 630.

444 Ryerson, F. J., Durham, W. B., Cherniak, D. J., and Lanford, W. A. (1989) Oxygen diffusion
445 in olivine: effect of oxygen fugacity and implications for creep. Journal of
446 Geophysical Research: Solid Earth, 94, 4105–18, doi: 10.1029/JB094iB04p04105.

447 Saikia, A., Ballaran, T., and Frost, D. (2009) The effect of Fe and al substitution on the
448 compressibility of $MgSiO_3$-perovskite determined through single-crystal x-ray
449 diffraction. Physics of the Earth and Planetary Interiors, 173, 153–161, doi:
450 10.1016/j.pepi.2008.11.006.

451 Sano, A., Ohtani, E., Kondo, T., Hirao, N., Sakai, T., Sata, N., Ohishi, Y., and Kikegawa, T.
452 (2008) Aluminous hydrous mineral δ-AlOOH as a carrier of hydrogen into the
453 core-mantle boundary. Geophysical Research Letters, 35, L03303, doi:
454 10.1029/2007gl031718.

455 Sano, A., Ohtani, E., Kubo, T., and Funakoshi, K. (2004) In situ X-ray observation of
456 decomposition of hydrous aluminum silicate $AlSiO_3OH$ and aluminum oxide

457 hydroxide δ-AlOOH at high pressure and temperature. Journal of Physics and
458 Chemistry of Solids, 65, 1547–1554, doi: 10.1016/j.jpcs.2003.12.015.

459 Sun, S. (1982) Chemical composition and origin of the Earth's primitive
460 mantle. Geochimica Et Cosmochimica Acta, 46, 179–192, doi:
461 10.1016/0016-7037(82)90245-9.

462 Suzuki, A. (2010) High-pressure X-ray diffraction study of epsilon-FeOOH. Physics and
463 Chemistry of Minerals, 37, 153–157, doi: 10.1007/s00269-009-0319-x.

464 Wänke, H., Dreibus, G. (1984) Mantle chemistry and accretion history of the Earth. In:
465 Kröner A, Hanson G, Goodwin A (eds) Archaean Geochemistry. Springer, Berlin, pp
466 l–24.

467 Xu, C., and Inoue T. (2019a) Melting of Al-rich phase D up to the uppermost lower mantle
468 and transportation of H_2O to the deep Earth. Geochemistry, Geophysics, Geosystems,
469 20, 4382–4389, doi: 10.1029/2019GC008476.

470 Xu, C., and Inoue T. (2019b) Phase relations in MAFSH system up to 21 GPa: implications
471 for water cycles in Martian interior. Minerals, 9, 559, doi: 10.3390/min9090559.

472 Xu, C., Nishi, M., and Inoue T. (2019) Solubility behavior of δ-AlOOH and ε-FeOOH at
473 high pressures. American Mineralogist, 104, 1416–1420, doi: 10.2138/am-2019-7064.

474 Xu, C., Steeve Gréaux, Inoue, T., Noda, M., Sun, W., and Kuwahara, H., et al. (2020)
475 Sound velocities of Al-bearing phase D up to 22 GPa and 1300 K. Geophysical
476 Research Letters, 47(18), doi: 10.1029/2020GL088877.

477 Yang, H., Prewitt, C. T., and Frost, D. J. (1997) Crystal structure of the dense hydrous
478 magnesium silicate, phase D. American Mineralogist, 272, 315–333, doi:
479 10.1016/S0040-1951(96)00265-X.

480 **Table 1**. Experimental run conditions and observed phase assemblages in the α-FeOOH-$Mg_{1.11}Si_{1.89}O_6H_{2.22}$ and
481 AlOOH-α-FeOOH-$Mg_{1.11}Si_{1.89}O_6H_{2.22}$ systems.

P (GPa)	T (°C)	Results	
		15.0 wt% α-FeOOH + $Mg_{1.11}Si_{1.89}O_6H_{2.22}$	8.0 wt% α-FeOOH + $Mg_{1.11}Si_{1.89}O_6H_{2.22}$
25	1600	St+Melt	St+Melt
25	1400	Brg+α-Fe_3O_2+St+Melt	Brg+St+Melt
25	1200	PhD+α-Fe_3O_2	PhD+α-Fe_3O_2
21*	1500*	Gt+Egg+St+Melt	Gt+St+Melt
21*	1300*	PhD+Melt (T)	PhD+α-Fe_3O_2+Melt (T)
21	1300	rw+St+Melt	rw+St+Melt
21	1100	PhD+α-Fe_3O_2+Melt	rw+PhD+St+Melt
20	1100	PhD+α-Fe_3O_2+Melt	rw+PhD+St+Melt
18	1000	rw (T)+PhD+α-Fe_3O_2+Melt	rw (T)+PhD+Melt

482 *Starting compositions are MORB and pyrolite-type.

483 PhD-phase D, St-stishovite, Brg-bridgmanite, Egg-phase Egg, Gt-garnet, rw-ringwoodite, T-trace amounts.

484 The duration times of heating at 1100-1400 °C and 1500-1600 °C are 60 and 20 minutes, respectively.

This is the peer-reviewed, final accepted version for American Mineralogist, published by the Mineralogical Society of America.
The published version is subject to change. Cite as Authors (Year) Title. American Mineralogist, in press.
DOI: https://doi.org/10.2138/am-2021-7907. http://www.minsocam.org/

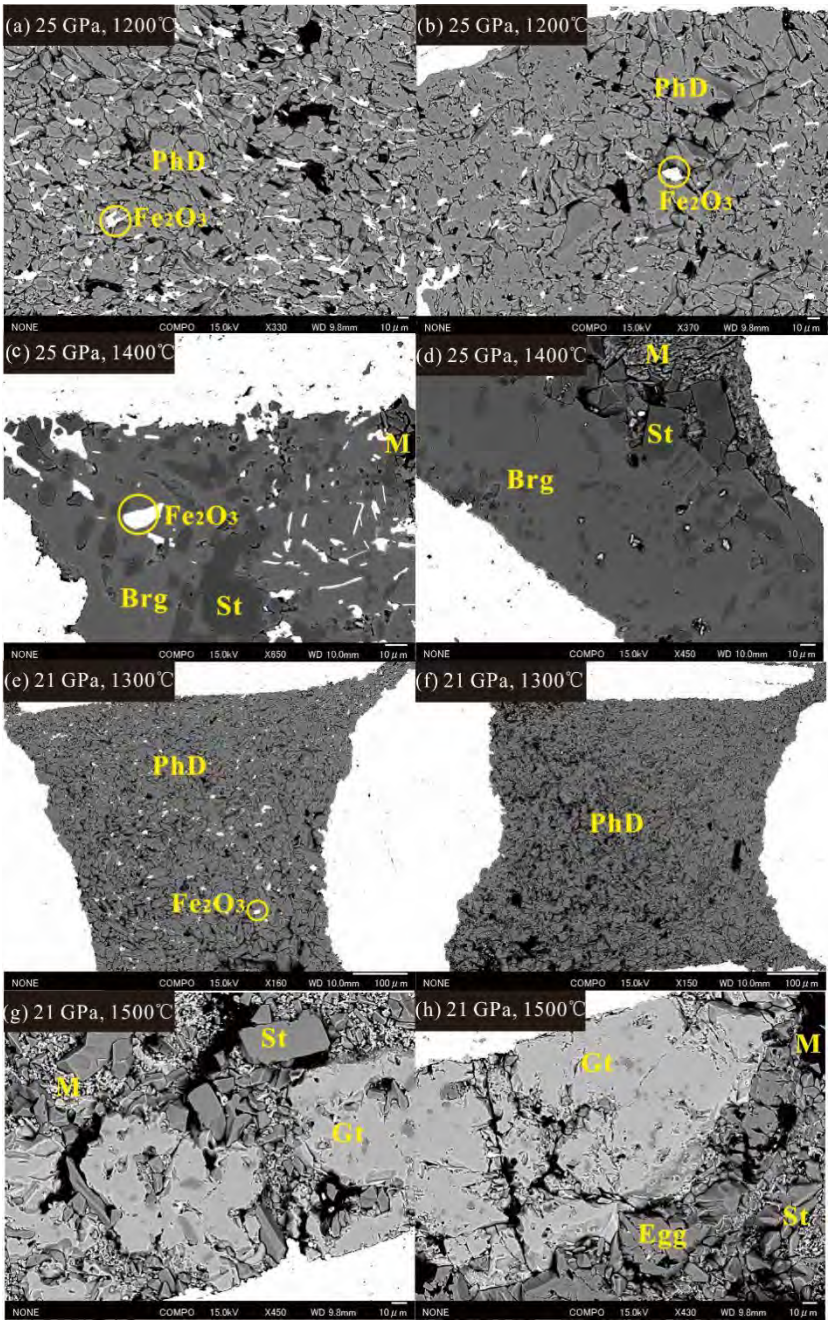

485

486 **Figure 1.** BSE images of representative run products (PhD-phase D, St-stishovite,
487 Brg-bridgmanite, Egg-phase Egg, M-melt, Gt, garnet) for samples synthesized at 25 GPa
488 and 1200 ºC with 15.0 wt% (a) and 8.0% wt% (b) of α-FeOOH + $Mg_{1.11}Si_{1.89}O_6H_{2.22}$; 25
489 GPa and 1400 ºC with 15.0 wt% (c) and 8.0% wt% (d) of α-FeOOH +
490 $Mg_{1.11}Si_{1.89}O_6H_{2.22}$; 21 GPa and 1300 ºC in pyrolite (e) and MORB-type (f) composition;
491 and 21 GPa and 1500 ºC in pyrolite (g) and MORB-type (h) composition.

This is the peer-reviewed, final accepted version for American Mineralogist, published by the Mineralogical Society of America.
The published version is subject to change. Cite as Authors (Year) Title. American Mineralogist, in press.
DOI: https://doi.org/10.2138/am-2021-7907. http://www.minsocam.org/

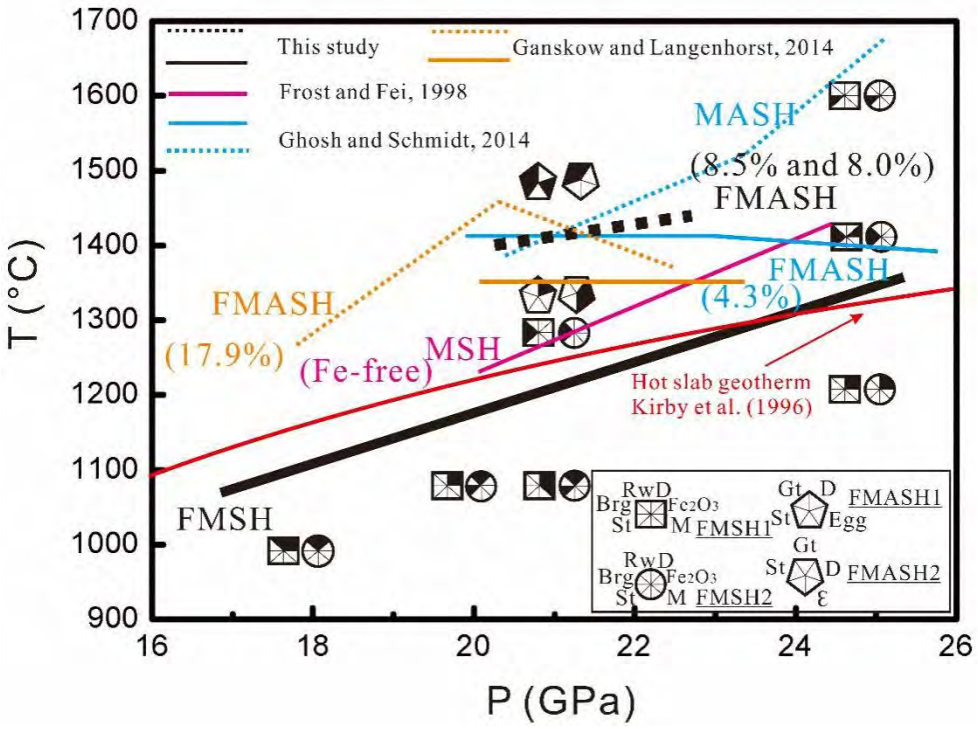

492

493 **Figure 2.** Phase diagram of PhD. MASH, MgO-Al_2O_3-SiO_2-H_2O. FMSH,
494 MgO-FeO/Fe_2O_3-SiO_2-H_2O. FMASH, MgO-Al_2O_3-FeO/Fe_2O_3-SiO_2-H_2O. The numbers 1
495 and 2 refer to high and low Al_2O_3 and FeO/Fe_2O_3 contents, respectively. The numbers in
496 parentheses represent the FeO/Fe_2O_3 content in a given starting composition. The stability
497 limit of Fe^{3+}-bearing PhD with both high and low Fe^{3+} contents is illustrated by the black
498 solid line, which is slightly lower than that of Mg-PhD (pink solid line) (Frost and Fei,
499 1998), and much lower than that for the Fe^{2+}-rich starting composition (yellow solid line)
500 (Ganskow and Langenhorst, 2014). The stability limit of Al, Fe^{3+}-bearing PhD in both
501 pyrolite and MORB-type composition is illustrated by the black dash line, which is much
502 higher than that of Fe^{3+}-bearing PhD. The trend of black dash line at high pressure is
503 possibly between the blue dash line in MASH and the blue solid line in FMASH (Ghosh
504 and Schmidt, 1998). However, Ganskow and Langenhorst (2014) observed different
505 behaviors of PhD in FMASH (yellow dash line). Hot slab geotherm from Kirby et al.
506 (1996) is plotted as a reference, e.g. 1200 °C at 660 km and 1300 °C at 820 km.

This is the peer-reviewed, final accepted version for American Mineralogist, published by the Mineralogical Society of America.
The published version is subject to change. Cite as Authors (Year) Title. American Mineralogist, in press.
DOI: https://doi.org/10.2138/am-2021-7907. http://www.minsocam.org/

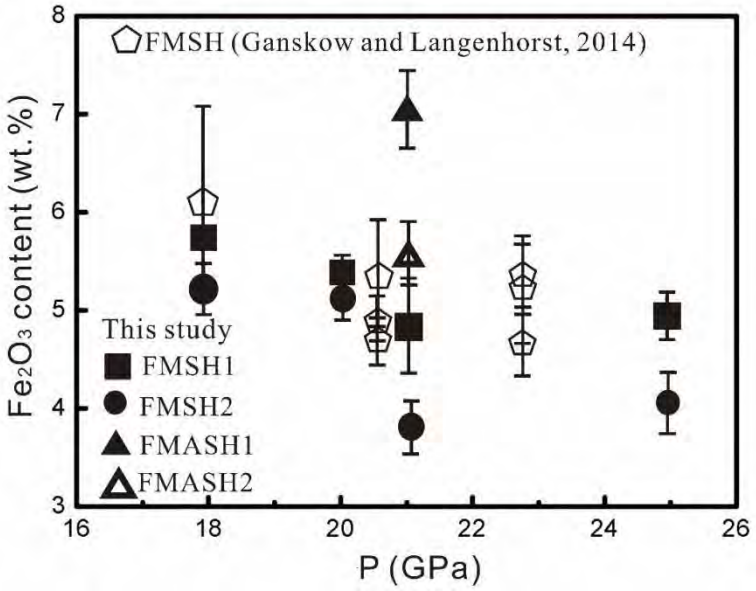

507

508 **Figure 3.** Variation of the Fe_2O_3 content in PhD as a function of pressure. Error bars are
509 2-sigma. The Fe_2O_3 content displays a decreasing trend with increasing pressure from 18 to
510 21 GPa; afterwards, it slightly increases to 25 GPa if ignore the uncertainties due to its
511 small crystalline size. This trend is consistent with that obtained by Ganskow and
512 Langenhorst (2014).

This is the peer-reviewed, final accepted version for American Mineralogist, published by the Mineralogical Society of America.
The published version is subject to change. Cite as Authors (Year) Title. American Mineralogist, in press.
DOI: https://doi.org/10.2138/am-2021-7907. http://www.minsocam.org/

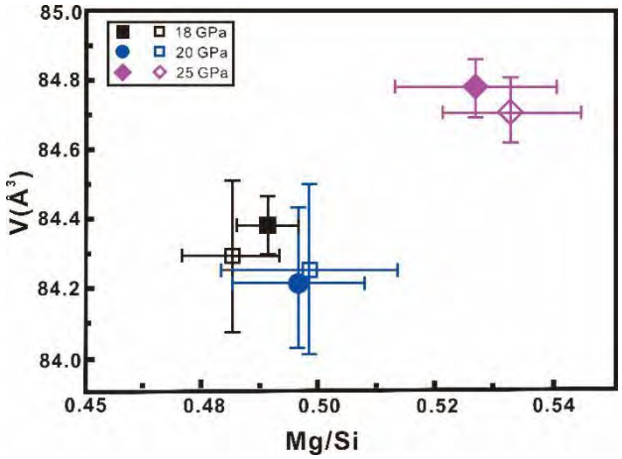

Figure 4. Relationship between the unit-cell volume and Mg/Si ratio of PhD at different pressures. Error bars are 2-sigma. Solid and open symbols refer to 15.0 wt% α-FeOOH + $Mg_{1.11}Si_{1.89}O_6H_{2.22}$ and 8.0 wt% αFeOOH + $Mg_{1.11}Si_{1.89}O_6H_{2.22}$, respectively. Obviously, different volume-Mg/Si relations exist at pressures of 18 - 20 GPa and 25 GPa. This is probably caused by different substitution mechanisms of Fe^{3+} in PhD. Between 18 and 20 GPa, the Tschermak-type substitution occurs in both Mg and Si sites ($Mg^{2+} + Si^{4+} = 2Fe^{3+}$). Thus, the decrease of Fe^{3+} content leads to a decrease in volume. By contrast, Fe^{3+} only occupies the Si site at elevated pressures ($Si^{4+} = Fe^{3+} + H^{+}$), thereby leading to an increase in volume even with a low Fe_2O_3 content.